Human Molecular Genetics, 2022, Vol. 31, 24, 4143–4158
https://doi.org/10.1093/hmg/ddac160
Advance access publication date 21 July 2022
Original Article

Clock genes rescue *nphp* mutations in zebrafish

Nicolas Kayser[1,†], Friedemann Zaiser[1,†], Anna C. Veenstra[1,†], Hui Wang[1,†], Burulca Göcmen[2], Priska Eckert[1], Henriette Franz[3], Anna Köttgen[2], Gerd Walz[1,4] and Toma A. Yakulov[1,*]

[1]Renal Division, University Freiburg Medical Center, Faculty of Medicine, Hugstetter Str. 55, Freiburg 79106, Germany
[2]Institute of Genetic Epidemiology, Faculty of Medicine and Medical Center, University of Freiburg, Freiburg 79106, Germany
[3]Department of Biomedicine, University of Basel, Pestalozzistr. 20, Basel CH-4056, Switzerland
[4]Signalling Research Centres BIOSS and CIBSS, University of Freiburg, Albertstrasse 19, Freiburg 79104, Germany

*To whom correspondence should be addressed. Tel: +49 76127063036; Email: toma.antonov.yakulov@uniklinik-freiburg.de

†The authors wish it to be known that, in their opinion, the first four authors should be regarded as joint First Authors.

Abstract

The zebrafish pronephros model, using morpholino oligonucleotides (MO) to deplete target genes, has been extensively used to characterize human ciliopathy phenotypes. Recently, discrepancies between MO and genetically defined mutants have questioned this approach. We analyzed zebrafish with mutations in the *nphp1-4-8* module to determine the validity of MO-based results. While MO-mediated depletion resulted in glomerular cyst and cloaca malformation, these ciliopathy-typical manifestations were observed at a much lower frequency in zebrafish embryos with defined *nphp* mutations. All *nphp1-4-8* mutant zebrafish were viable and displayed decreased manifestations in the next (F2) generation, lacking maternal RNA contribution. While genetic compensation was further supported by the observation that *nphp4*-deficient mutants became partially refractory to MO-based *nphp4* depletion, zebrafish embryos, lacking one *nphp* gene, became more sensitive to MO-based depletion of additional *nphp* genes. Transcriptome analysis of *nphp8* mutant embryos revealed an upregulation of the circadian clock genes *cry1a* and *cry5*. MO-mediated depletion of *cry1a* and *cry5* caused ciliopathy phenotypes in wild-type embryos, while *cry1a* and *cry5* depletion in maternal zygotic *nphp8* mutant embryos increased the frequency of glomerular cysts compared to controls. Importantly, *cry1a* and *cry5* rescued the nephropathy-related phenotypes in *nphp1*, *nphp4* or *nphp8*-depleted zebrafish embryos. Our results reveal that *nphp* mutant zebrafish resemble the MO-based phenotypes, albeit at a much lower frequency. Rapid adaption through upregulation of circadian clock genes seems to ameliorate the loss of *nphp* genes, contributing to phenotypic differences.

Graphical Abstract

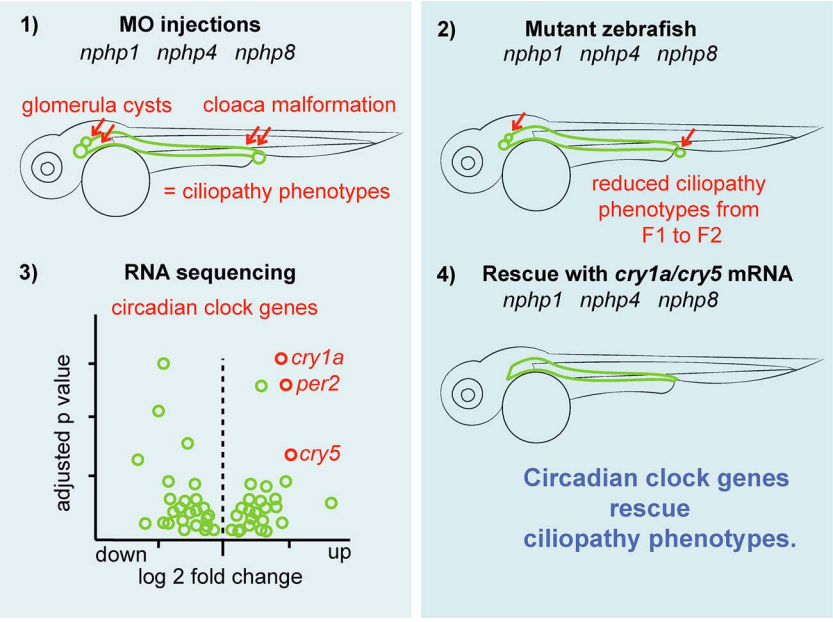

Received: May 16, 2022. **Revised:** July 6, 2022. **Accepted:** July 8, 2022

Introduction

Nephronophthisis (NPH) is the most common cause of hereditary kidney failure in children. NPH is a heterogenetic condition, caused by mutations in more than 20 different genes. Most NPH gene products (NPHPs) localize to the cilium, and therefore NPH is considered a ciliopathy. The spectrum of manifestations is highly variable with overlap to other syndromic diseases. Most NPH patients suffer from renal failure that leads to end-stage renal disease within the first two decades of life. The kidneys of NPH patients are typically characterized by cysts at the cortico-medullary junction and an interstitial inflammation. The extrarenal manifestations encompass cerebellar abnormalities such as a vermis aplasia, blindness caused by retinitis pigmentosa, *situs inversus*, liver fibrosis and cardiac defects. Two other disease entities, the Joubert syndrome (JBTS) and Meckel-Gruber syndrome (MKS) share genetic and phenotypic overlap with NPH.

Based on physical interactions and overlapping functions, NPHP and MKS family members have been grouped in distinct protein modules (1), including the NPHP1-4-8, the NPHP2-3-9/AHII, the NPHP5-6/Ataxin10 and the MKS1-6/Tectonic2 module. While the NPHP1-4-8 module, interacting with polarity proteins, has been linked to the apical organization and polarity of epithelial cells, the NPHP5-6 and MKS1-6 modules seem to control ciliary integrity and hedgehog signaling, respectively.

The ciliated sensory neurons of *Caenorhabditis elegans* have been extensively studied to characterize the molecular function of NPHPs (2–6). Genetic manipulation of the *C. elegans* homologues revealed a hierarchy of MKS and NPH family members that recruit proteins to the ciliary compartment, form the transition zone and initiate ciliogenesis. MKS-5 (RPGRIP1L/NPHP8) plays a central role in anchoring MKS and NPHP protein modules (7), while NPHP-2 (INVS/NPHP2) is partially redundant with NPHP-1 and NPHP-4, and not required for the localization of NPHP and MKS proteins to the ciliary transition zone (8).

The analysis of molecular functions of NPHPs in mammalian animal models has been more complex. While biallelic *NPHP1* mutations are a common cause of hereditary renal failure in children (9), deletion of mouse *Nphp1* only results in male infertility and retinal degeneration, but no other ciliopathy phenotypes (10). The *Nphp4*^{mmf192} mutant mouse line, generated by ethyl nitrosourea (ENU) mutagenesis, is predicted to truncate NPHP4 after amino acid 103 due to a nonsense mutation and insertion of a stop codon instead of a leucine at position 104 (11). Homozygous *Nphp4*$^{mmf192/mmf192}$ mice exhibit a normal life-span and no renal abnormalities, but develop photoreceptor degeneration and reduced sperm motility (11). Biallelic *RPGRIP1L/NPHP8* mutations are associated with severe disease manifestations in humans (12,13), and deletion of *Nphp8* in mice results in embryonal lethality (14), underlining the central role of NPHP8.

It has been known for some time that the circadian clock is an important regulator of renal physiological functions (15,16). Although many genes comprise the circadian clock in mammals, four form a feedback loop system to control the expression of *Period* (*Per* homologs 1, 2 and 3) and *Cryptochrome* (*Cry* homologs 1 and 2) (17). The expression of *Bmal1*, *Clock*, *Per1* and *Cry2* in the kidney follows a clear 48-h rhythm (18). The circadian clock genes have been previously implicated in the pathophysiology of renal diseases such as chronic kidney disease and hypertension (19–22); however, their *involvement* in ciliopathies is unknown.

The translucent zebrafish embryo represents a genetic tractable model system to characterize the effects of gene mutations, and knockdown of NPHP homologues in zebrafish embryos has been extensively used to elucidate the cellular and molecular functions of NPH family members. Using *nphp* mutant zebrafish generated by ENU mutagenesis screens or targeted gene deletion, we analyzed the disease manifestations caused by mutations within the *nphp1–nphp4–nphp8* module. We found that zebrafish with Nphp truncations were viable, and ciliopathy phenotypes observed in the first generation were progressively lost in subsequent generation. Furthermore, mutant zebrafish embryos displayed resistance against morpholino oligonucleotide (MO)-mediated gene depletion, suggesting genetic compensation. RNA sequencing (RNAseq) and functional studies identified the circadian clock genes *cry1a* and *cry5* as components of the compensatory mechanisms in the *nphp8* mutant zebrafish.

Results

Ciliopathy phenotypes in zebrafish lines with defined *nphp* point mutations

To counteract deleterious gene mutations, zebrafish displays an amazing capacity to compensate the loss of gene functions (23–25). We therefore decided to characterize zebrafish *nphp* mutant lines, and determine how ciliopathy phenotypes change over time. Screening the Sanger Institute (https://www.sanger.ac.uk/) and European Zebrafish Resource Center (https://www.ezrc.kit.edu/index.php), we identified zebrafish lines with *nphp4* and *nphp8* mutations that resulted in a premature stop or eliminated essential splice sites (ESSs) (Supplementary Material, Fig. S1); no zebrafish lines with *nphp1* mutations have been identified. We therefore targeted exon 15 of zebrafish *nphp1* to generate the *nphp1*$^{ex15\text{-}del4}$ mutant zebrafish line. The *nphp1*$^{ex15\text{-}del4}$ mutation affected amino acid 454 with a stop at amino acid 463, eliminating the C-terminal 213 amino acids of zebrafish Nphp1 (Supplementary Material, Table S1). To compare the impact of the *nphp* mutations on disease manifestations, we quantified two typical ciliopathy phenotypes, glomerular cysts and cloaca malformation. Heterozygote +/*nphp1*$^{ex15\text{-}del4}$ crosses

resulted in a normal Mendelian ratio at 6 and 30 days post fertilization (Fig. 1A). Homozygote mutant (m/m) zebrafish embryos, analyzed 48hours post fertilization (hpf), showed a significant increase in glomerular cysts and cloaca malformation (Fig. 1B). Similarly, the frequency of glomerular cyst formation was increased in mutant zebrafish. Heterozygote (+/m) zebrafish had an intermediate frequency of glomerular and cloaca cyst formation, suggesting some degree of haplotype insufficiency; however, the differences between wild-type (+/+) and (+/m) zebrafish were statistically not significant. To eliminate the maternal contribution, homozygote *nphp1*$^{ex15\text{-}del4}$ zebrafish of the F1 generation were crossed to generate maternal zygotic (m/m) zebrafish (F2 generation); the (+/+) siblings of this cross were used as controls (Supplementary Material, Fig. S1D). Elimination of the maternal contribution had no striking effect on glomerular cysts or cloaca malformation. In fact, the F2 generation became indistinguishable from their wild-type siblings with a very low frequency of abnormalities (Fig. 1B and C).

In the zebrafish *nphp4*^{sa38686} line, a G > A mutation eliminates an ESS at amino acid 764 (Supplementary Material, Fig. S1B). Heterozygote +/*nphp4*^{sa38686} crosses resulted in a normal Mendelian ratio (Supplementary Material, Table S1). Homozygote mutant (m/m) zebrafish embryos, analyzed 48 hpf, showed no apparent ciliopathy phenotype (Fig. 2A). To eliminate the maternal contribution, homozygote *nphp4*$^{sa38686/sa38686}$ zebrafish of the F1 generation were crossed to generate maternal zygotic (m/m) zebrafish (F2 generation); the (+/+) siblings of this cross were used as controls. In comparison with wild-type siblings, the F2 generation developed ciliopathy phenotypes at a higher frequency (Fig. 2B and Supplementary Material, Fig. S2), but a comparison between the F1 and F2 generation, analyzing the total number of combined glomerular and cloaca cysts, did not reveal significant differences between the F1 and F2 generation (Fig. 2C).

The zebrafish *nphp4*^{sa41188} line contains a nonsense mutation (G > T) that replaces amino acid 444 by a stop codon (Supplementary Material, Fig. S1B). Heterozygote +/*nphp4*^{sa41188} crosses resulted in a normal Mendelian ratio (Supplementary Material, Table S1). Homozygote mutant (m/m) zebrafish embryos, analyzed 48 hpf, showed no apparent increase in cloaca malformation, but a statistically significant increase in glomerular cyst formation by more than 8-fold in comparison with wild-type (+/+) zebrafish embryos (Fig. 3A). While maternal zygotic *nphp4*$^{sa41188/sa41188}$ (m/m) zebrafish (F2 generation) displayed several ciliopathy phenotypes (Supplementary Material, Fig. S2), the frequency of glomerular cyst formation declined to 4.9-fold, and was no longer statistically different from (+/+) siblings (Fig. 3B). The frequency of cloaca malformation increased moderately, but did not reach statistical significance. Thus, the F2 *nphp4*^{sa41188} generation was statistically no longer different from wild-type siblings. The comparison between the F1 and F2 generation and analyzing the total number of combined glomerular and cloaca cysts, revealed a significant reduction of abnormalities in the F2 generation (Fig. 3C).

To eliminate most of the zebrafish *nphp4*, exon 1 was targeted by CRISPR/Cas9 to generate the *nphp4*$^{ex1\text{-}del5}$ zebrafish line. This mutation alters the reading frame at amino acid 16, resulting in a premature stop after 44 amino acids (Supplementary Material, Fig. S1B and Supplementary Material, Table S1). Crossing of heterozygote +/*nphp4*$^{ex1\text{-}del5}$ seemed to increase glomerular cysts and cloaca malformation; however, the overall frequency was low and the differences were statistically not significant (Fig. 3D). Generation of homozygote *nphp4*$^{ex1\text{-}del5}$ (m/m) F2 zebrafish to eliminate maternal contribution increased the number of cloaca malformation in comparison with wild-type siblings, but not the number of glomerular cysts (Fig. 3E). Other ciliopathy phenotypes such as abnormalities of the body axis were identical between wild-type siblings and homozygote *nphp4*$^{ex1\text{-}del5}$ (m/m) F2 zebrafish (Fig. 3F). The combined number of glomerular and cloaca cyst formation declined slightly from the homozygote *nphp4*$^{ex1\text{-}del5}$ (m/m) F1 to the F2 generation (Fig. 3G). Thus, despite removal of most of the zebrafish *nphp4* gene, homozygote *nphp4* $^{ex1\text{-}del5}$ zebrafish were viable and ciliopathy-associated phenotypes were limited to an increase in cloaca malformation in the F2 generation.

The zebrafish *nphp8*^{sa10096} line contains a nonsense mutation (T > A) at amino acid 849, which truncates the protein at the end of the C2 domain (Supplementary Material, Fig. S1C and Supplementary Material, Table S1). Heterozygote +/*nphp8*^{sa10096} crosses resulted in a normal Mendelian ratio (Supplementary Material, Table S1). Homozygote *nphp8*^{sa10096} (m/m) zebrafish embryos, analyzed 48 hpf, showed statistically significant increases in cloaca malformation and glomerular cysts formation in comparison with wild-type (+/+) zebrafish embryos (Fig. 4A). Heterozygote (+/m) zebrafish embryos displayed an intermediate increase in glomerular cysts and cloaca malformation, but both changes were statistically not significant. The maternal zygotic (m/m) mutant zebrafish embryos displayed several ciliopathy phenotypes (Supplementary Material, Fig. S3), including an increase in glomerular and cloaca cyst formation in comparison with their wild-type (+/+) siblings (Fig. 4B). Comparison between the F1 and F2 generation, taken the combined frequency of abnormalities into account, revealed a decline of glomerular cyst and cloaca malformation (Fig. 4C).

Similar changes were observed for the *nphp8*^{sa24730} mutation. In *nphp8*^{sa24730} zebrafish mutants, an ESS at amino acid 337 is eliminated by an A > T mutation (Supplementary Material, Fig. S1C and Supplementary Material, Table S1). Heterozygote +/*nphp8*^{sa24730} crosses resulted in a normal Mendelian ratio (Supplementary Material, Table S1). Homozygote mutant

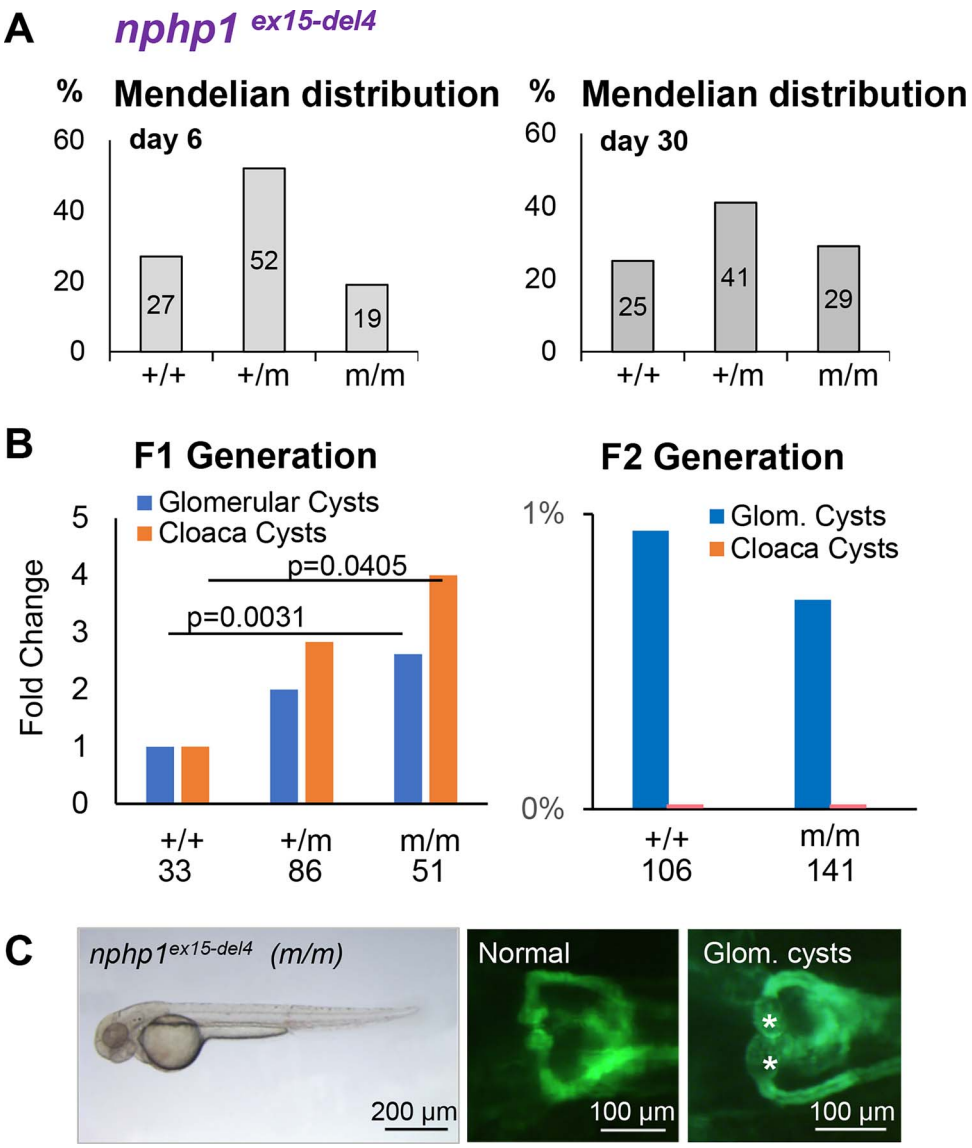

Figure 1. Characterization of *nphp1*-deficient zebrafish. (**A**) Exon 15 of zebrafish *nphp1* was targeted by CRISPR/Cas9 to generate the *nphp1*$^{ex15\text{-}del4}$ mutant zebrafish. Analysis at 6 and 30 days post fertilization revealed normal Mendelian distributions after incross of heterozygotic *nphp1*$^{+/ex15\text{-}del\ 4}$ zebrafish, revealing that *nphp1*-deficient zebrafish is viable. The number of embryos per genotype is depicted inside the bars. (**B**) Heterozygote (+/m) and homozygote (m/m) mutants showed a progressive increase in glomerular and cloaca cyst formation in comparison with wild-type zebrafish (Fisher's exact test, two-tailed). However, the F2 generation of homozygote *nphp1*-deficient zebrafish [*nphp1*$^{ex15\text{-}del4}$ (m/m)] did not develop more glomerular cysts or cloaca malformation in comparison with their wild-type siblings. The numbers displayed below the graph depict the group size. (**C**) While *nphp1*$^{ex15\text{-}del4}$ (m/m) zebrafish embryos displayed a normal body axis, occasional glomerular cysts were detectable at 48 hpf. The asterisks (∗) mark the glomerular cysts.

(m/m) zebrafish embryos, analyzed 48 hpf, showed statistically significant increases in cloaca malformation in comparison with wild-type (+/+) zebrafish embryos, while both homozygote (m/m) and heterozygote (+/m) zebrafish embryos displayed significantly more glomerular cysts in comparison with wild-type (+/+) zebrafish embryos (Fig. 4D). While maternal zygotic (m/m) zebrafish embryos displayed several ciliopathy phenotypes (Supplementary Material, Fig. S3) with a significant increase in cloaca malformation, glomerular cyst formation was no longer different from wild-type (+/+) siblings (Fig. 4E). Comparison between the F1 and F2 generation revealed a decline of combined glomerular cyst and cloaca malformation similar to the *nphp8*^{sa10096} mutation (Fig. 4F). Thus, both *nphp8* mutations are associated with a significant increase in glomerular cyst and cloaca malformations that is ameliorated in subsequent generations. Compound heterozygotic zebrafish, resulting from crosses between the *nphp1*, *nphp4* and *nphp8* maternal zygotic zebrafish mutants (m/m) did not display an increased frequency of ciliopathy phenotypes in comparison with heterozygotic (+/m) controls (Supplementary Material, Fig. S4).

Ciliopathy-related phenotypes in zebrafish can often be attributed to defective ciliary structure or function. Immunofluorescence using anti-acetylated Tubulin antibody revealed increased incidence of disorganized cilia in the proximal straight and the distal early tubules

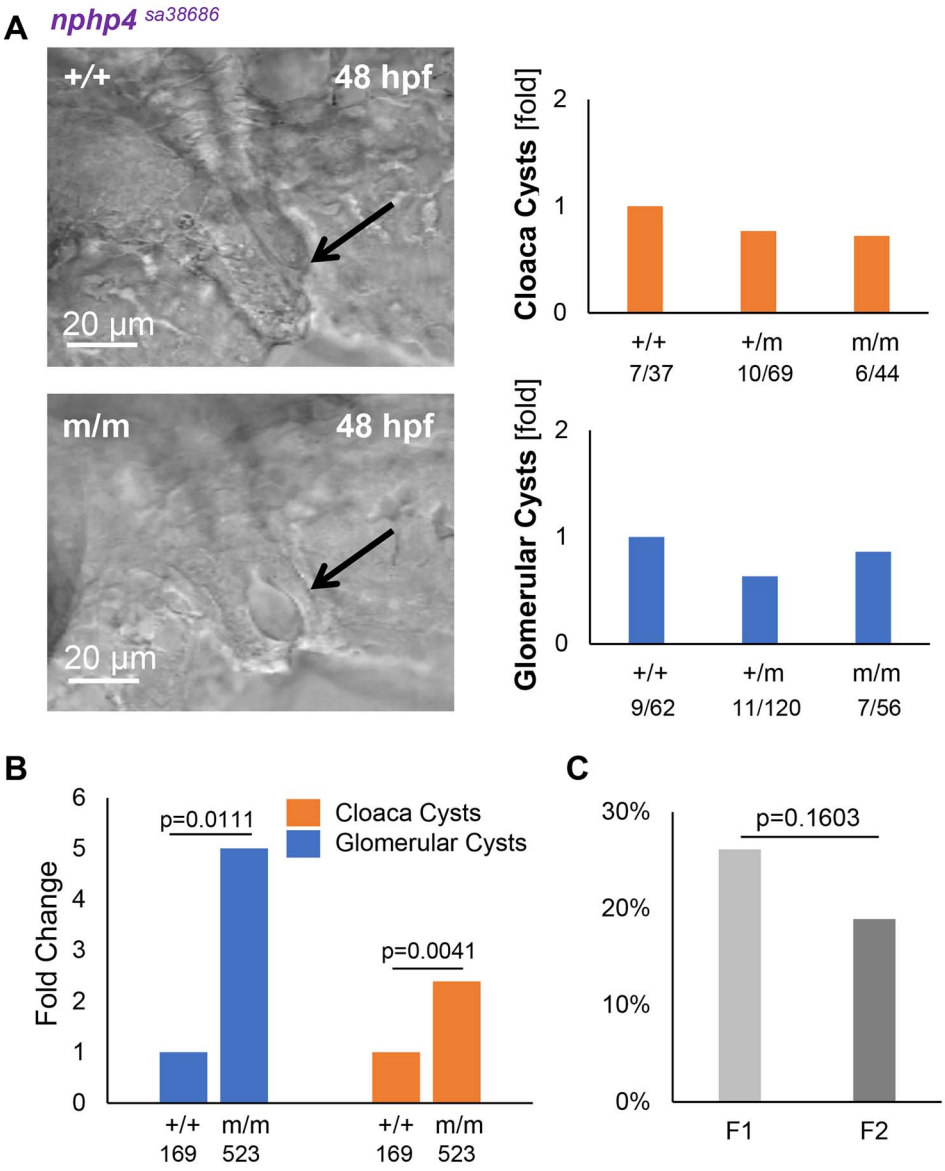

Figure 2. Maternal zygotic *nphp4*^{sa38686} *(m/m)* zebrafish mutants display an increase in cyst formation. (**A**) Crossing of heterozygote +/*nphp4*^{sa38686} did not increase glomerular cysts or cloaca malformation. The left images depict typical examples of normal (+/+) and defective cloaca formation (m/m) in zebrafish embryos at 48 hpf, visualized by DIC microscopy. The arrows point to a normally developed cloaca (upper panel) and a cloaca cyst (bottom panel). The numbers below the graphs depict the fraction of embryos with cysts and the total number of analyzed embryos. (**B**) Crossing of homozygote *nphp4*^{sa38686} (m/m) zebrafish resulted in a 5-fold increase in glomerular and in a 2-fold increase in cloaca cyst formation in homozygote (m/m) maternal zygotic zebrafish embryos in comparison with wild-type (+/+) siblings (Fisher's exact test, two-sided). The numbers displayed below the graph depict the group size. (**C**) The combined number of glomerular and cloaca cyst formation declined slightly from the *nphp4*^{sa38686} (m/m) F1 to the F2 generation (Fisher's exact test, two-sided).

of the *nphp8*^{sa24730} and *nphp1*$^{ex15\text{-}del4}$ homozygous mutants compared to controls (Supplementary Material, Fig. S5). The pronephric cilia of homozygous *nphp4*$^{ex1\text{-}del5}$ larvae appeared mostly normal (Supplementary Material, Fig. S5), which is consistent with the milder phenotypes observed in this zebrafish line.

Resistance and susceptibility to MO-mediated gene depletion in *nphp* mutant zebrafish embryos

We next analyzed the impact of MO-mediated knockdown in the *nphp4*^{sa38686} and *nphp4*^{sa41188} mutant zebrafish lines, using *nphp4* splice (SBM)- and translation-blocking (TBM) MOs. MOs increased cloaca malformation moderately in wild-type siblings (+/+), while glomerular cyst formation increased by more than 50-fold (Fig. 5). While the maternal zygotic mutants (m/m) displayed a higher incidence of glomerular cyst and cloaca malformation at baseline, the response to MOs was strongly reduced in mutant zebrafish, suggesting the absence of functional Nphp4 protein in the *nphp4*^{sa38686} and *nphp4*^{sa41188} mutant zebrafish.

We next tested the susceptibility of *nphp* mutants in response to the depletion of additional *nphp* genes.

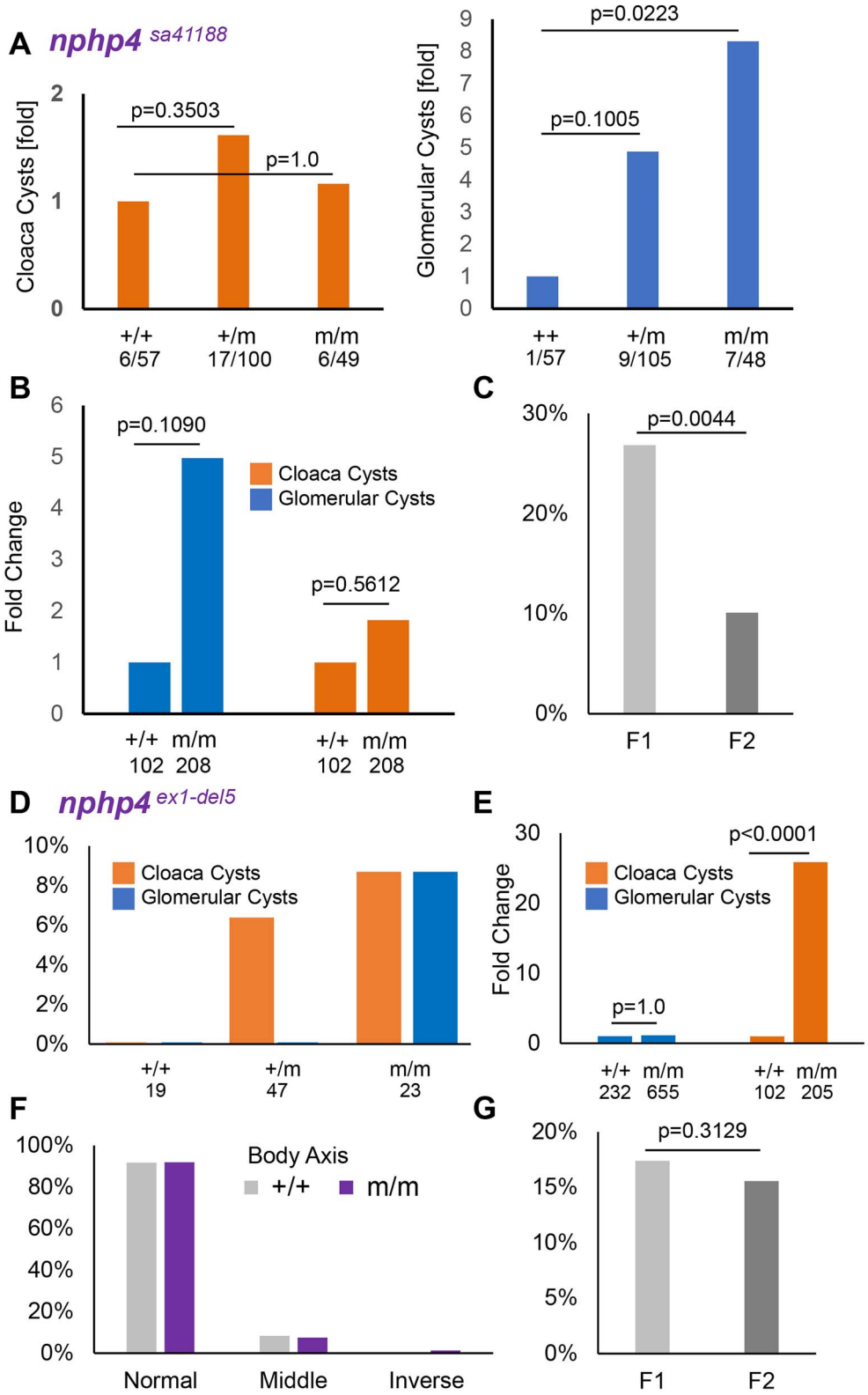

Figure 3. Characterization of *nphp4*^{sa41188} and *nphp4*$^{ex1\text{-}del5}$ mutant zebrafish lines. (**A**) While homozygote *nphp4*^{sa41188} (m/m) zebrafish did not experience an increased frequency of cloaca malformation, the number of glomerular cysts was significantly increased (Fisher's exact test, two-sided). (**B**) The homozygotic (m/m) in-cross (F2 generation) showed a moderate increase in glomerular cyst and cloaca malformation that was statistically not significant. (**C**) The combined number of glomerular and cloaca cyst formation declined significantly from the *nphp4*^{sa41188} (m/m) F1 to the F2 generation (Fisher's exact test, two-sided). (**D**) Crossing of heterozygote +/*nphp4*$^{ex1\text{-}del5}$ zebrafish did not result in a significant increase in either glomerular cysts or cloaca malformation. (**E**) Generation of homozygote *nphp4*$^{ex1\text{-}del5}$ (m/m) F2 zebrafish increased the number of cloaca malformation in comparison with wild-type siblings, but not the number of glomerular cysts. (**F**) Other ciliopathy phenotypes such as abnormalities of the body axis, were comparable between wild-type siblings and homozygote *nphp4*$^{ex1\text{-}del5}$ (m/m) F2 zebrafish. (**G**) The combined number of glomerular and cloaca cyst formation declined slightly from the *nphp4*$^{ex1\text{-}del5}$ (m/m) F1 to the F2 generation; however, the difference was statistically not significant (Fisher's exact test, two-sided). The numbers displayed below the graphs depict the group size.

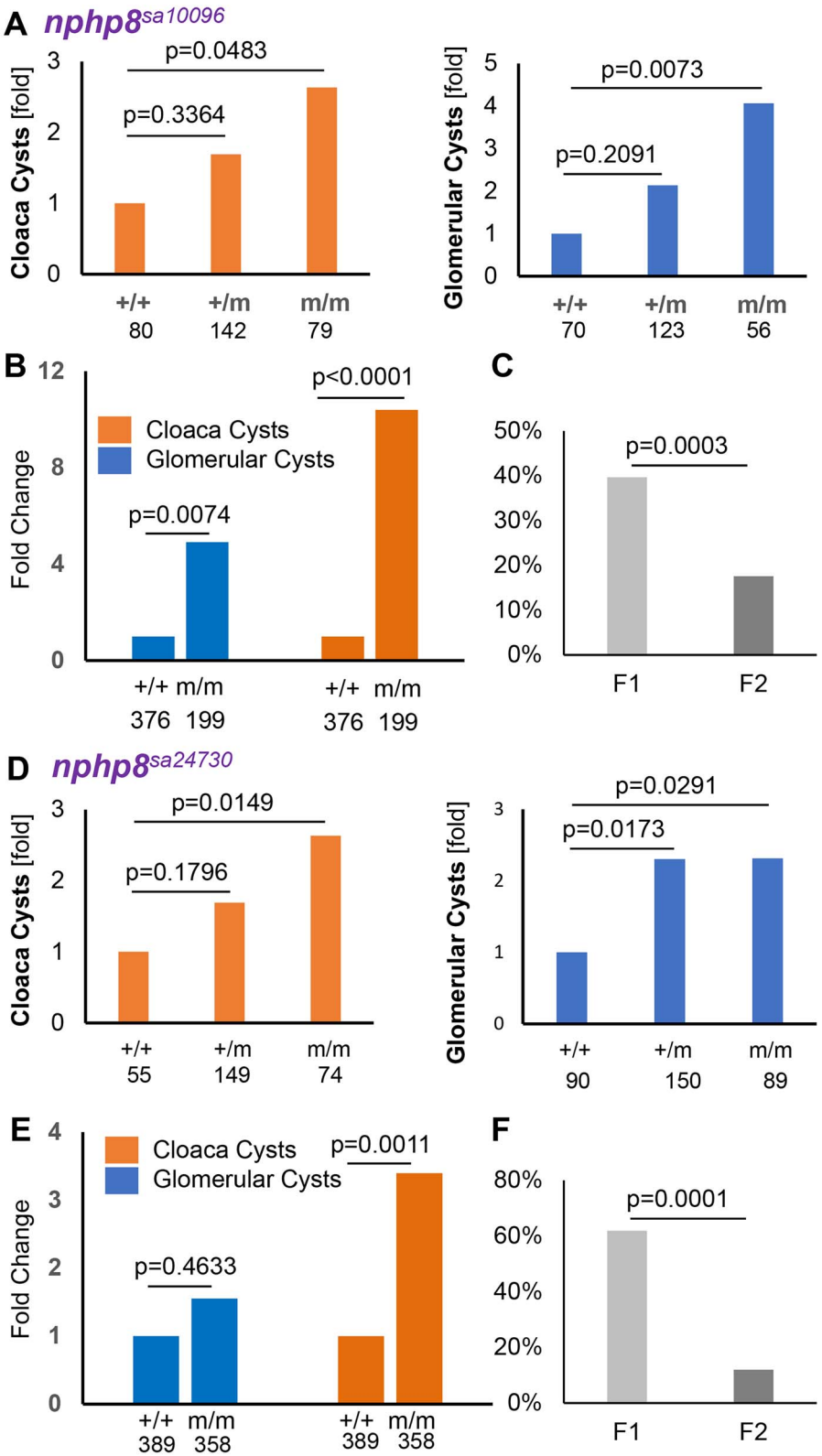

Figure 4. Characterization of *nphp8*^{sa10096} and *nphp8*^{sa24730} mutant zebrafish lines. (**A**) Homozygote *nphp8*^{sa10096} (m/m) zebrafish displayed an increased frequency of cloaca malformation and glomerular cysts. (**B**) The homozygotic (m/m) incross (F2 generation) showed an increase in glomerular cyst and cloaca malformation. (**C**) The combined number of glomerular and cloaca cyst formation declined significantly from the *nphp8*^{sa10096} (m/m) F1 to the F2 generation. (**D**) Heterozygote *nphp8*^{sa24730} (+/m) and homozygote *nphp8*^{sa24730} (m/m) zebrafish displayed an increased frequency of cloaca malformation and glomerular cysts. (**E**) While glomerular cyst formation was not more frequent between wild-type siblings and the mutant F2 generation (m/m), cloaca malformation increased significantly. (**F**) Comparison between the F1 and F2 generation, combining glomerular cyst and cloaca malformation, revealed a decline of combined glomerular cyst and cloaca malformation similar to the *nphp8*^{sa10096} mutation. The number of examined embryos is depicted below the graphs. All *P* values were calculated, using the two-sided Fisher's exact test.

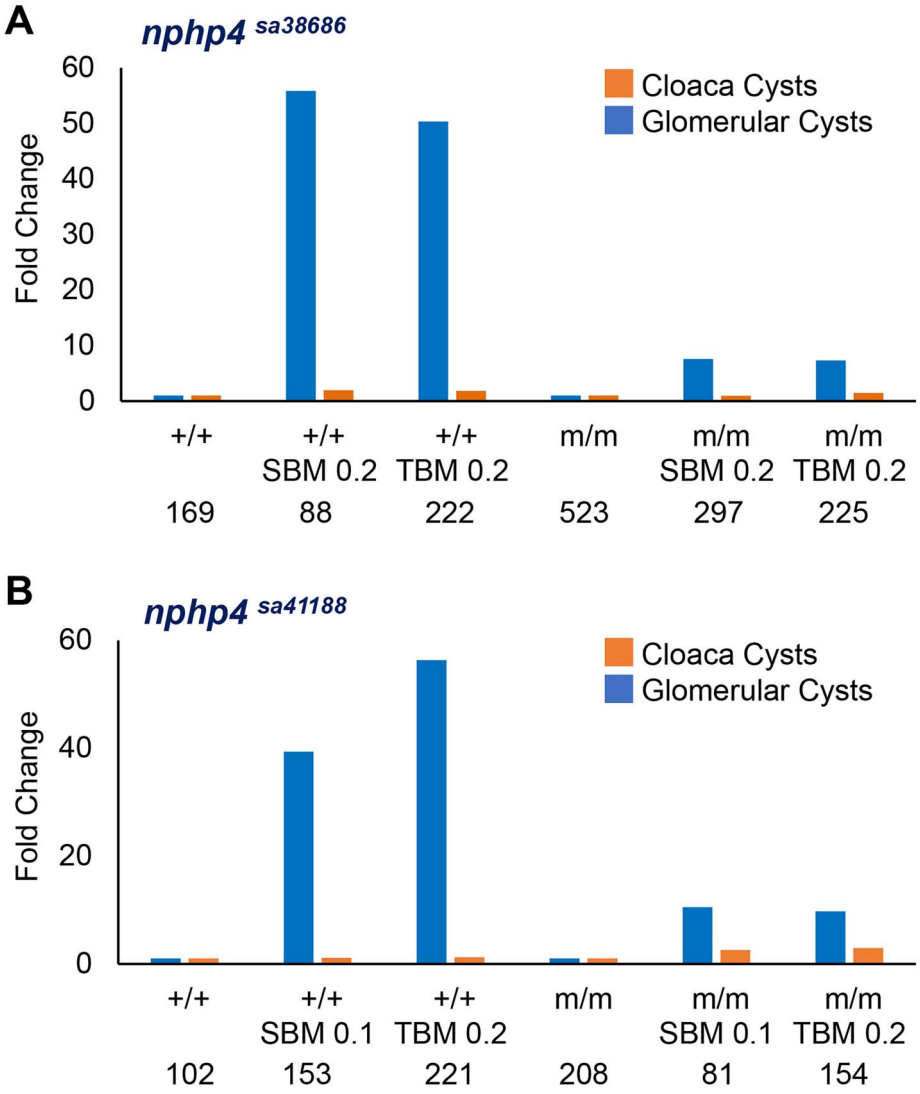

Figure 5. Resilience of *nphp4* mutant zebrafish lines against MO-mediated *nphp4* depletion. Wild-type siblings (+/+) or homozygote nphp4 mutants (m/m) zebrafish embryos were treated with SBM or TBM (0.1 or 0.2 mM). Glomerular cyst and cloaca malformation were expressed as fold change in relationship to control MO-injected zebrafish embryos (0.2 mM). While wild-type siblings remained sensitive to either SBM or TBM and primarily developed glomerular cysts, mutant zebrafish displayed a blunted response, suggesting resistance to MO-mediated *nphp4* depletion. The numbers displayed below the graph depict the respective group size.

Depletion of *nphp8* with TBM increased the frequency of glomerular cysts and cloaca malformation in *nphp4*^{sa41188} (m/m) zebrafish in comparison with *nphp4*^{sa41188} (+/+) siblings (Fig. 6A and B). Additional depletion of *nphp4* with TBM (0.2 mM) in the *nphp8*^{sa24730} mutant zebrafish embryos slightly increased the frequency of glomerular cysts, but had no effect on cloaca malformation (Fig. 6C and D).

Identification of the circadian clock genes *cry1a* and *cry5* as components of the compensatory mechanism in the *nphp8* mutant zebrafish

Both the *nphp8*^{sa10096} and *nphp8*^{sa24730} mutations displayed a marked decrease in glomerular cysts and cloaca malformation over subsequent generations (Fig. 4), implying the existence and activation of compensatory mechanisms that could rescue the ciliopathy-associated phenotypes. To uncover these mechanisms, we compared the transcriptional profiles of 2-day-old maternal zygotic homozygous *nphp8*^{sa24730} mutant larvae and control siblings by RNAseq. RNAseq revealed that the *nphp8*^{sa24730} mutation caused a deletion of seven base pairs in the 5′ of exon 8, leading to a frameshift followed by 60 missense base pairs and a premature stop codon (Supplementary Material, Fig. S6A). Using DESeq2 (26), we identified 1034 differentially expressed genes (Supplementary Material, Table S2). Gene ontology (GO) analysis revealed significant enrichment for GO terms associated with the circadian clock (Supplementary Material, Fig. S6B, Supplementary Material, Table S3). Among the top 10 genes upregulated in the *nphp8*^{sa24730} mutants were *cry1a*, *cry5* and *per2* (Fig. 7A, Supplementary Material, Table S2), which are all part of the circadian clock gene network (27,28). To determine whether *cry1a* and *cry5* are

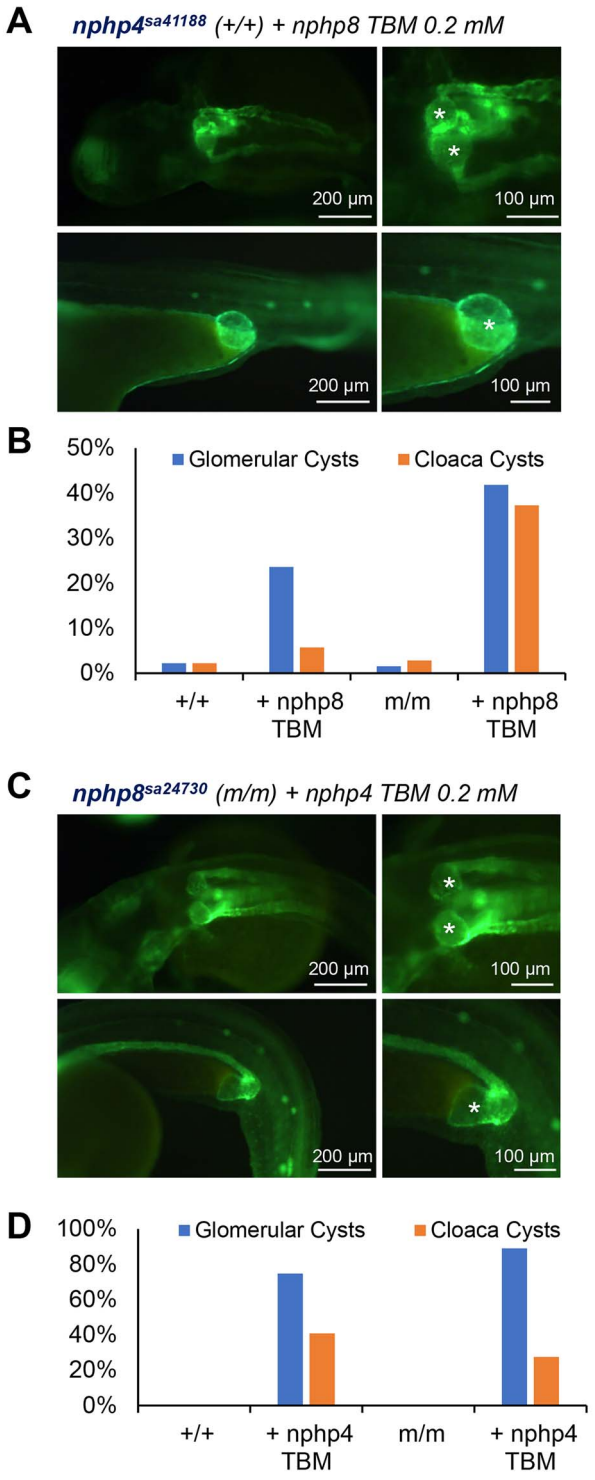

Figure 6. Susceptibility of *nphp* mutants in response to depletion of additional *nphp* genes. (**A**) Zebrafish *nphp4*^{sa41188} (+/+) siblings developed glomerular cysts and cloaca malformation (asterisks) after depletion of *nphp8* with TBM (0.2 mM). (**B**) While the *nphp4*^{sa41188} in-cross (F2 generation) (m/m) was viable and displayed very little ciliopathy-specific phenotypes, additional depletion of *nphp8* with TBM (0.2 mM) increased the frequency of glomerular cysts and cloaca malformation in comparison with *nphp4*^{sa41188} (+/+) siblings. (**C**) Zebrafish *nphp8*^{sa24730} (m/m) developed glomerular cysts and cloaca malformations (asterisks) after depletion of *nphp4* with TBM (0.2 mM). (**D**) The *nphp8*^{sa24730} in-cross (F2 generation) (m/m) was viable and displayed very little ciliopathy-specific phenotypes. Additional depletion of *nphp4* with TBM (0.2 mM) slightly increased the frequency of glomerular cysts, but had little effect on cloaca malformation.

linked to the ciliopathy-related phenotypes, we depleted *cry1a* and *cry5* in *Tg(cdh17:GFP; wt1b:GFP)* embryos with sSBM and TBM. Both *cry1a* TBM and SBM caused a significant increase in the frequency of glomerular cyst formation (Fig. 7B). Cloaca malformations were also increased in response to the *cry1a* SBM, but to a lesser extent; the *cry1a* TBM had no effect on the cloaca development. Depletion of *cry5* with SBM and TBM showed a similar effect: the frequency of glomerular cyst and cloaca malformation was significantly increased compared to controls (Fig. 7B). Depletion of *cry1a* and *cry5* with MOs also significantly increased the frequency of laterality defects, heart edema, hydrocephalus and body curvature in 2-day-old zebrafish larvae (Supplementary Material, Fig. S7). Immunofluorescence with anti-acetylated Tubulin antibody revealed that the proximal straight and distal early tubules of *cry1a* and *cry5*-depleted 2-day-old larvae were more often dilated and displayed disordered cilia compared to controls (Supplementary Material, Fig. S8). These results indicate that *cry1a* and *cry5* are part of the ciliopathy-related gene network. Quantitative RT-PCR (qRT-PCR) revealed that cry1a and cry5 are also upregulated in the *nphp1* and *nphp4* homozygous (m/m) zebrafish mutants (Supplementary Material, Fig. S9). To understand whether the upregulation of *cry1a* and *cry5* might have a compensatory function, we used MOs to deplete *cry1a* and *cry5* in the *nphp8*^{sa24730} mutants. *cry1a* SBM-mediated knockdown significantly increased the glomerular cyst malformation in the maternal zygotic *nphp8*^{sa24730} larvae (Fig. 7C), whereas the effect of the *cry1a* TBM was more subtle. Similarly, both the *cry5* SBM and TBM almost doubled the frequency of glomerular cyst malformation (Fig. 7C), while cloaca malformations did not occur. Thus, our results indicate that the circadian clock genes *cry1a* and *cry5* are part of the compensatory gene network to compensate the detrimental effects of *nphp8* ^{sa24730} mutation.

cry1a and *cry5* rescue *nphp1-4-8* depletion in zebrafish

Depletion of cilia-associated molecules by antisense MOs has been extensively used to characterize the function of ciliopathy genes. Depletion of the three zebrafish *nphps*, using a TBM at concentrations between 0.2 and 0.4 mM resulted in glomerular cyst formation within the proximal segment of the pronephros, ranging from 9 to 36% of the analyzed embryos (Fig. 8). Cloaca malformation, manifesting as a cyst instead of the normal distal body opening, ranged from 2 to 31%, and was primarily observed in *nphp4*-depleted zebrafish embryos, consistent with the published observations (29,30). The lowest frequency of cloaca cysts was observed in *nphp1*-depleted zebrafish embryos. Either *cry1a* or *cry5* mRNA alone rescued the ciliopathy-related phenotypes after *nphp1* depletion, and resulted in a reduction, albeit not a statistically significant one, in cloaca and glomerular cysts in *nphp4* or *nphp8*-depleted embryos (Fig. 8). Importantly,

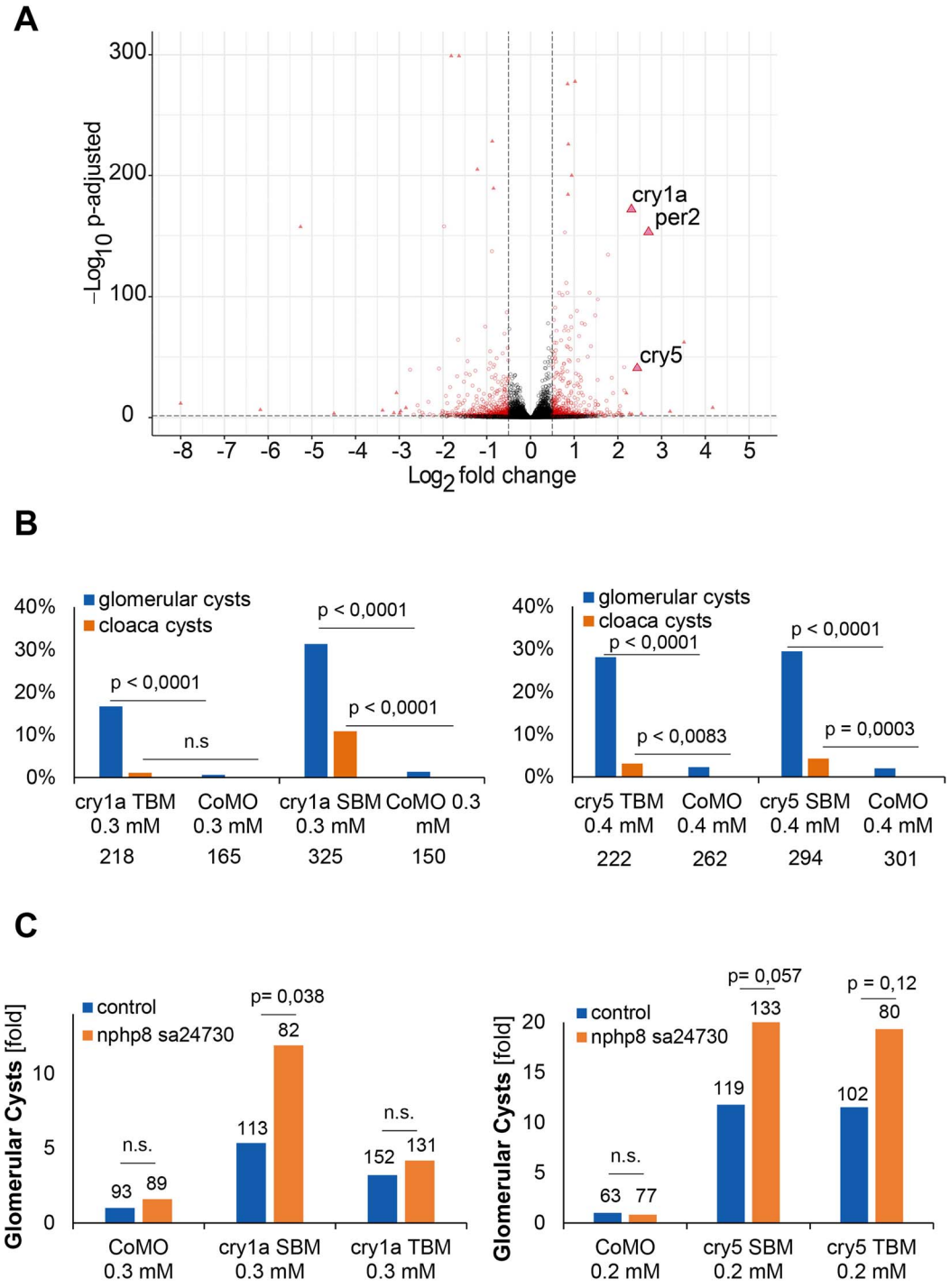

Figure 7. Circadian clock genes are part of the *nphp8* genetic network controlling the ciliopathy-specific phenotypes. (**A**) Differential expression studies of *nphp8*^{sa24730} mutants and control siblings identified the circadian clock genes *cry1a*, *cry5* and *per2* as upregulated in the *nphp8* mutants. (**B**) Depletion of *cry1a* and *cry5* in *Tg(wt1b:GFP; cdh17:GFP)* embryos with two different MO each (SBM and TBM) significantly increased the frequency of glomerular cyst malformations compared to control morpholinos. Cloaca malformations were also significantly increased, but to a lesser extent. The numbers below the graphs depict each group size. (**C**) Depletion of *cry1a* with SBM in the *nphp8*^{sa24730} in-cross (F2 generation) more than doubled the frequency of glomerular cyst formation in comparison with control siblings; depletion with *cry1a* TBM led to a slight, but not significant increase in glomerular cysts (left graph). Depletion of *cry5* with SBM or TBM in the *nphp8*^{sa24730} in-cross (F2 generation) almost doubled the frequency of glomerular cyst formation without reaching significance (defined by $P < 0.05$). Glomerular cysts were expressed as fold change in relationship to control MO-injected zebrafish embryos. The numbers above the graphs depict the group size. All *P*-values were calculated using Fisher's exact test.

cry1a and *cry5* together rescued the cloaca and glomerular cyst formation in *nphp1*, *nphp4* or *nphp8*-depleted embryos (Fig. 8), indicating that these clock genes are part of the compensatory mechanism in zebrafish.

Discussion

Defined *nphp* mutations produce ciliopathy phenotypes

NPHP4 mutations cause End Stage Renal Disease (ESRD) with a variable onset (6–35 years), often associated with retinitis pigmentosa (31). Elimination of an ESS in zebrafish *nphp4*^{sa38686}, predicted to truncate Nphp4 at amino acid 764, was not associated with glomerular cyst or cloaca malformation, while a nonsense mutation, inserting a stop codon at amino acid 444 revealed an increase in glomerular cyst formation that was statistically significant. In contrast, neither glomerular cyst nor cloaca malformation of maternal zygotic *nphp4*$^{sa38686/sa38686}$ zebrafish mutants were statistically different from wild-type embryos. Mutations in *NPHP8/RPGRIP1L* were identified in patients with NPH, JBTS, MKS, COACH syndrome and retinitis pigmentosa, encompassing a broad spectrum of disease manifestations (cerebello-oculo-renal malformations). Homozygote truncating *NPHP8* mutations are typically associated with embryonal lethal forms of MKS, consistent with *Nphp8*-deficient mice (13). Zebrafish embryos with a truncating mutation at amino acid 862 (*nphp8*^{sa10096}) were viable and fertile, but revealed an increase in glomerular cyst and cloaca malformation, resembling the severity of the mammalian phenotype. While the increase of glomerular cyst and cloaca malformation was not significant in heterozygote zebrafish embryos, glomerular cyst formation reached statistically significance for heterozygote *nphp8*^{sa24730} zebrafish embryos, a line with a deletion of an ESS that truncates Nphp8 presumably at amino acid 337. Heterozygote *Nphp8/Rpgrip1l*$^{+/-}$ mice develop adiposity (32–35), supporting the hypothesis that haplotype insufficiency may contribute to mammalian disease manifestations.

Amelioration of phenotypes in the F2 generation

All analyzed zebrafish mutant lines were vital and fertile, permitting the generation and analysis of maternal zygotic mutants devoid of any maternal mRNA contribution (F2 generation). In the *nphp4*$^{sa41188/sa41188}$ zebrafish line the F1 generation displayed a significant increase in glomerular cyst formation, but differences become non-significant in the F2 generation. It appears that zebrafish *nphp* mutations that leave most of the protein intact, are not consistently associated with ciliopathy phenotypes in the F1 generation. In contrast, zebrafish embryos with more severe truncating mutations display significant phenotypes; however, these phenotypes can be partially compensated in the F2 generation, while phenotypes worsen in zebrafish embryos with less severe mutations. Human *NPHP8* mutations are often associated with extensive disease manifestations; in fact, biallelic truncating mutations typically result in a full-blown MKS and embryonal lethality. Both *nphp8* mutations resulted in significant glomerular cyst and cloaca malformation in the F1 generation, and only the frequency of glomerular cyst formation declined in the F2 generation of the *nphp8*^{sa24730} mutation, suggesting that defective Nphp8 function in zebrafish is less well compensated than the loss of other *nphps*.

Circadian clock genes and genetic compensation in *nphp8* mutants

The RNAseq screen identified multiple genes involved in the circadian clock that were upregulated in *nphp8*^{sa24730} zebrafish mutants. Although *cry1a*, *cry5* and *per2* were among the top 10 upregulated genes, other clock genes such as *cry3b*, *per1b* and *per3* also displayed significantly higher expression levels in the *nphp8* mutants (Supplementary Material, Table S3). Our functional studies demonstrated that *cry1a* and *cry5* depletion can cause ciliopathy-related phenotypes in zebrafish. Importantly, *cry1a* and *cry5* can at least partially compensate for the loss of *nphp8*. The compensation mechanism most likely involves downstream target genes of the circadian oscillator. Studies from mammals have highlighted the role of circadian clock genes in the regulation of kidney-specific gene expression and function. Mouse deficient for CRY1 and CRY2 displayed a significant reduction in the circadian aldosterone oscillations, and transcriptome analysis of the adrenal glands of these mice detected an increase in expression of the aldosterone biosynthetic enzyme 3β-hydroxysteroid dehydrogenase/delta 5-to-4 isomerase type 6 (36). PER1 has been shown to control the expression of genes involved in sodium reabsorption, including NCC, SGLT1, NHE3, WNK1, WNK4 and α-ENaC (37–41), and *Period 1*-deficient mice develop salt-sensitive, non-dipping hypertension (42).

Ciliopathy phenotypes caused by MO-mediated knockdown of *nphp* family are rescued by circadian clock genes

MO-mediated knockdown has been an extensively utilized tool to analyze the function of newly identified NPHPs in zebrafish embryos (43–50). Interference with ciliary functions results in ciliopathy phenotypes that can be readily quantified during the first 72 hpf, including glomerular cyst formation, abnormalities of the body axis and cloaca malformation; more elaborate manifestations entail the direct analysis of ciliary morphology and function (51). Additional, less specific abnormalities such as cardiac edema, hydrocephalus and deformed body curvature are often detected as the result of defective ciliary functions. Our findings were consistent with previous observations: knockdown of zebrafish *nphp1* predominantly results in glomerular cyst formation (30). The incidence of cloaca cyst formation was highest (>20%) after *nphp4* depletion with TBM

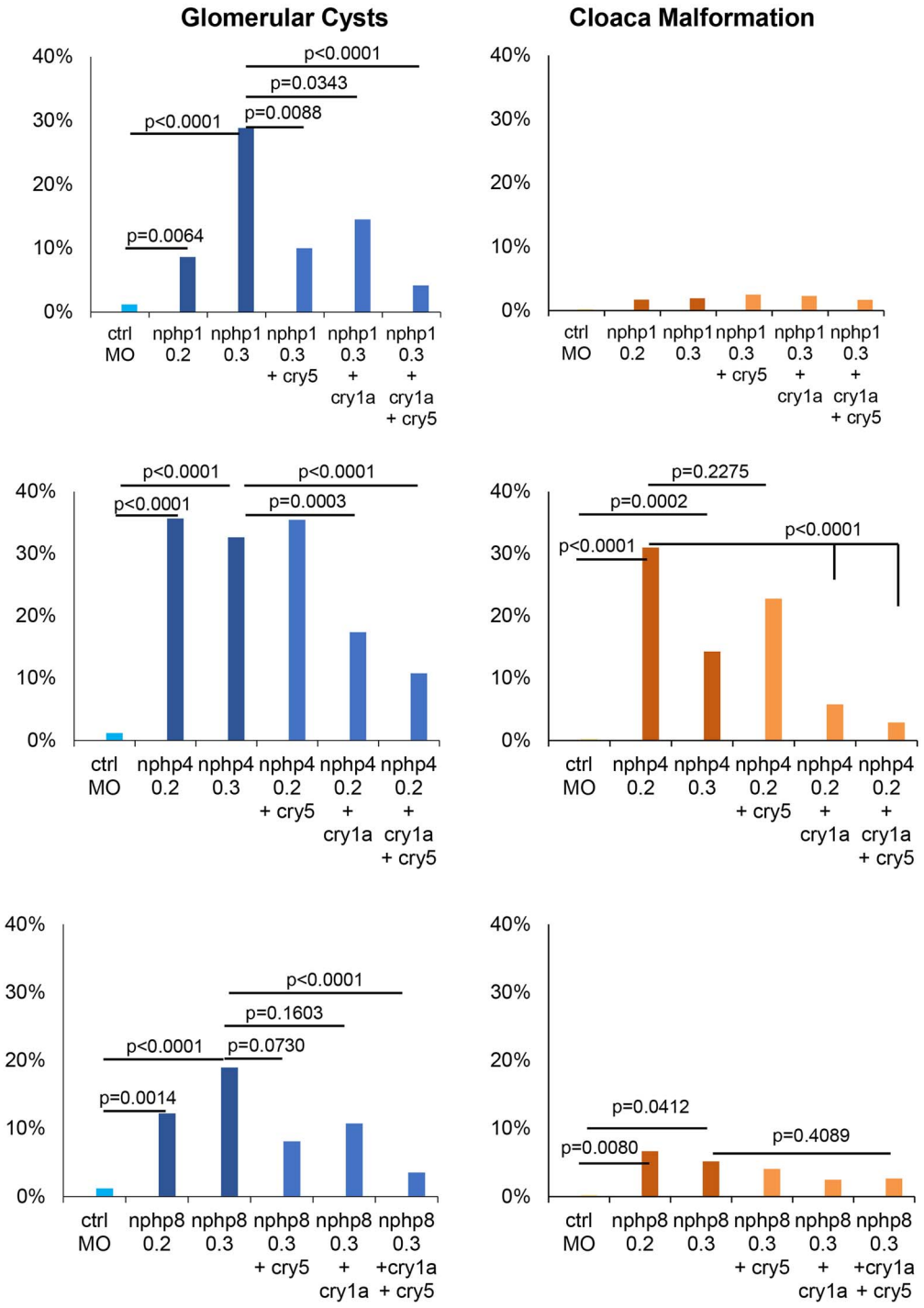

Figure 8. MO-mediated knockdown of the components of the nphp1-4-8 module. TBMs were used to deplete zebrafish *nphp1*, *nphp4* and *nphp8* as indicated. Glomerular cysts and cloaca malformation (cloaca cysts) were expressed in comparison with control MO-injected zebrafish embryos. The control represents the average of six independent control MO injections at concentrations between 0.2 and 0.4 mM. The MO concentrations (mM) are shown below the group names.

(29,30). Increases in glomerular cyst and cloaca malformation were also observed in *nphp8*-depleted zebrafish embryos. Although the efficacy of MOs cannot be compared directly, *nphp4* and *nphp8* depletion appear to cause more severe ciliopathy phenotypes in comparison with *nphp1* knockdown; in fact, MO-mediated knockdown of *nphp1* almost selectively triggers glomerular cysts, which is an agreement with a renal-limited disease in most human disease. Interestingly, the circadian clock genes *cry1a* and *cry5* rescued the *nphp1*, *nphp4* and *nphp8* MO-induced phenotypes. Together with the observation that circadian clock genes are upregulated

in the *nphp8* mutant zebrafish, our findings indicate that the circadian clock might be a part of the Nphp compensatory network.

Our analysis demonstrates that zebrafish lines with *nphp* nonsense mutations or elimination of ESSs display less extensive phenotypes in comparison with MO-depleted zebrafish embryos. Furthermore, maternal zygotic lines of all mutant zebrafish lines were viable. The resulting phenotypes in the F2 seemed to be disproportional to the severity of the mutation: while early truncating mutations caused significant phenotypes in the F1 generation, abnormalities became less prevalent in the F2 generation, and *vice versa*. Apparently, the developmental pressure to compensate genetic defects in zebrafish is higher in early truncating mutations. Since mRNA are still generated, decay-mediated generation of RNA fragments could facilitate compensation. Upregulation of *cry1a* and *cry5* in the $nphp8^{sa24730}$ mutants and their involvement in the development of ciliopathy-related phenotypes in zebrafish suggest compensatory mechanisms related to the circadian oscillator. The identification of genetic networks that compensate ciliopathy-associated defects in zebrafish may provide a new conceptual framework to ameliorate these rare but serious human hereditary diseases.

Materials and Methods

Zebrafish lines and maintenance

Zebrafish lines were raised and maintained as previously described (52). All zebrafish (*Danio rerio*) husbandry was performed under standard conditions in accordance with national ethical and animal welfare guidelines approved by the ethics committee for animal experiments at the Regierungspräsidium Freiburg, Germany (permit number G-16/89). The $nphp4^{sa38686}$, $nphp4^{sa41188}$, $nphp8^{sa10096}$ and $nphp8^{sa24730}$ zebrafish lines were obtained from the European Zebrafish Resource Center (EZRC), Karlsruhe, Germany. To visualize the pronephros, all lines were crossed into the double transgenic *Tg(cdh17:GFP; wt1b:GFP)* line (53). The lines $nphp4^{ex1\text{-}del5}$ and $nphp1^{ex15\text{-}del4}$ were generated in this study by CRISPR/Cas9-mediated mutagenesis. Guide RNAs (gRNAs) were designed using CHOPCHOP (http://chopchop.cbu.uib.no/) (54). A PCR-based strategy for the sgRNA template construction was used (55). gRNAs were synthesized using the MEGAshortscript T7 Transcription Kit (Thermo Fisher Scientific, Waltham, MA, USA). Purification was performed with the MONARCH RNA Cleanup Kit (New England Biolabs, Ipswich, MA, USA). gRNAs were injected together with Cas9 protein at the one-cell stage. The following gRNAs were used in this study: $nphp4^{ex1\text{-}del5}$ 5′-GTGTCACGTGAAGTCCATCG-3′ and $nphp1^{ex15\text{-}del4}$ 5′-AGTGTACCGTAGAGCAATGG-3′.

Comparison of the F1 with F2 generation

To compare the frequency of glomerular cyst and cloaca malformation between heterozygotic crosses (F1 generation) with homozygotic crosses (F2 generation), both phenotypes were combined. If phenotypes were acquired in separate experiments, the frequency of one phenotype was proportionally adjusted to the other phenotype.

MO-mediated knockdowns

MOs were obtained from Gene Tools, LLC, Philomath, OR, USA. MOs were diluted in 100 mM KCL, 10 mM 4- (2-hydroxyethyl)-1-piperazineethanesulfonic acid and 0.1% phenol red (Sigma-Aldrich). About 4 nl of this solution was microinjected into fertilized eggs at the one-cell stage. Embryos and larvae were kept at 28°C in Danieau's solution with 0.003% 1-phenyl-2-thiourea added at 24 hpf to avoid skin pigmentation. Antisense MOs were designed to target the translation start site (TBM) or an ESS (splice blocking MOs, SBM) of the respective genes. A standard control MO (5´-CCTCTTACCTCAGTTACAATTTATA-3′) was used as a control for all MO experiments. To reduce side effects, all MOs were co-injected with a p53-targeting MO (5´-GCGCCATTGCTTTGCAAGAATTG-3′) (56) The following MOs were used in this study:

nphp1-TBM 5′-CCCTCTTCTCTTTGGAGGCATGTTG-3′ (30).

nphp4-TBM 5′-GCGCTTCTCCACTCAGACATCAGAG-3′ (30).

nphp4-SBM 5′-ATTTATTCCCCATCCACCTGTGTCA.

nphp8-TBM 5′-TTAAGCGTGAGGTTTTCATCCTGCA-3′

nphp8-SBM 5′-TCTGTCAGTGCAGATTGAGTCACTC-3′ (57)

cry1a-TBM 5′-CAGTGGACTGTATTGACCACCATTA-3′

cry1a-SBM 5′-ATATTTGTCATCCGATCCCTTACCT-3′

cry5-TBM 5′-CTCCACAGAGTCTTCTGATTACGTG-3′

cry5-SBM 5′-CGCGCAGACTTTAAACTCCATACCT-3′

For the rescue experiments, *cry1a* and *cry5* were amplified from cDNA from 1–2-day-old zebrafish embryos, and were cloned in pCS2+ plasmid. mRNA was produced using T7 or Sp6 polymerase. About 4 nl of 50 ng/μl mRNA was co-injected with the respective MO.

Imaging and immunofluorescence

Embryos of the *Tg(cdh17:GFP; wt1b:GFP)* line were analyzed at 48–50 hpf under a Leica MZ16F epifluorescent microscope. Images were obtained with a Leica DFC 450C camera and processed with Leica Application Suite (Leica Microsystems, Wetzlar, Germany). Differential interference contrast (DIC) imaging was done with Zeiss LSM 880 NLO inverted microscope, using the C-Achroplan 40×/0.80 objective with water–oil as immersion medium (Carl Zeiss, Oberkochen, Germany). For imaging, embryos were embedded in 1% low-melting agarose and covered with Danieau's solution. Cilia were stained for immunofluorescence with primary mouse anti-acetylated Tubulin antibody (T6793, Sigma-Aldrich, St. Louis, MO, USA). The secondary antibody was Cy3-donkey anti-mouse IgG (715-165-50, Jackson ImmunoResearch, Ely, UK). Briefly, 2-day-old embryos were fixed

in 4% paraformaldehyde at 4°C overnight and stored in methanol at −20°C until needed. For immunofluorescence, embryos were equilibrated in phosphate-buffered saline with tween and triton (PBSTT) solution (0.1% Tween-20 and 0.1% Triton-X in PBS) for 30 min with frequent solution changes, digested for 20 min with Proteinase K (10 μg/ml). Blocking was performed in PBSTT supplemented with 1% DMSO, 2% sheep serum and 1% BSA for 1 h. primary antibody was applied overnight at room temperature and after 90 min wash in PBSTT with frequent solution changes, secondary antibody was applied overnight at room temperature. Confocal images were recorded with a C-Apochromat 40×/1.2 objective on an LSM 880 Observer confocal microscope (Carl Zeiss). Figures were prepared using Fiji (58).

Quantitative RT-PCR

qRT-PCR was performed as previously described (59). The following primers were used: β-actin (*actb1*), forward 5′-TGTGAGTTTTCAGTGCACGC-3′ and reverse 5′-TCCCATGCCAACCATCACTC-3′; *cry1a*, forward 5′-caggacgaggcttacacagc-3′ and reverse 5′-aaatcaggcctctgcgaagt-3′; *cry5*, forward 5′-caggtggactgggacaacaa-3′ and reverse 5′-cagccctcctgtcgtaactg-3′. The fold change was calculated by the $\Delta\Delta C_t$ method (where C_t is threshold cycle) using *actb1* as the housekeeping gene. The resulting values were compared with an unpaired Student's *t*-test.

RNAseq and data analysis

Total RNA from four biological replicates each from control and mutant zebrafish larvae was extracted, and sequenced by Eurofins Genomics, Konstanz, Germany on an Illumina sequencer as paired-end 150 bp reads. Using STAR 2.7.3a (60) with default parameters, the fastq files were aligned to zebrafish reference genome assembly GRCz11, with genome sequence and gene annotation files downloaded from Ensembl release 104. Quantification of gene expression was performed using RSEM v1.3.1 (61), and transcripts per kilobase million (TPM) values were generated per gene and sample. Differential gene expression analysis was performed with the DESeq2 (1.30.1) package in R, with alpha = 0.05 used to generate the results (26). GO term enrichment analysis was performed using enrichGO function from clusterProfiler (3.18.1) package (45). Mutant splice site of *nphp8* mutants was visualized using Integrative Genomics Viewer (2.10.3) (62). Volcano plot was generated using the EnhancedVolcano package in R (https://github.com/kevinblighe/EnhancedVolcano).

Supplementary Material

Supplementary Material is available at *HMG* online.

Acknowledgements

We are grateful to Mrs Annette Schmitt and Mrs Carina Kramer for the technical support and all members of our laboratory for helpful discussions. We thank the staff of the aquatic core facility (AquaCore) at the University Freiburg Medical Center—IMITATE, Germany for the excellent support with the zebrafish maintenance and experimentation. We would like to thank the Life Imaging Center at the University Freiburg, Germany for expert support.

Conflict of Interest statement: The authors declare no conflict of interest.

Data availability

The RNA sequencing data is deposited at GEO (GSE206983) and is available for download at https://www.ncbi.nlm.nih.gov/geo/query/acc.cgi?acc=GSE206983.

Funding

This work was funded by the Deutsche Forschungsgemeinschaft (DFG, German Research Foundation) CRC 850—project A7 (awarded to G.W.), CRC 1453—Project-ID 431984000 (awarded to G.W. and T.A.Y.), and under Germany's Excellence Strategy—EXC-2189—Project ID: 390939984 (awarded to G.W.).

References

1. Sang, L., Miller, J.J., Corbit, K.C., Giles, R.H., Brauer, M.J., Otto, E.A., Baye, L.M., Wen, X., Scales, S.J., Kwong, M. *et al.* (2011) Mapping the NPHP-JBTS-MKS protein network reveals ciliopathy disease genes and pathways. *Cell*, **145**, 513–528.
2. Otto, E., Kispert, A., Schätzle, S., Lescher, B., Rensing, C. and Hildebrandt, F. (2000) Nephrocystin: gene expression and sequence conservation between human, mouse, and *Caenorhabditis elegans*. *JASN*, **11**, 270–282.
3. Wolf, M.T.F., Lee, J., Panther, F., Otto, E.A., Guan, K.-L. and Hildebrandt, F. (2005) Expression and phenotype analysis of the nephrocystin-1 and nephrocystin-4 homologs in *Caenorhabditis elegans*. *JASN*, **16**, 676–687.
4. Jauregui, A.R. and Barr, M.M. (2005) Functional characterization of the *C. elegans* nephrocystins NPHP-1 and NPHP-4 and their role in cilia and male sensory behaviors. *Exp. Cell Res.*, **305**, 333–342.
5. Williams, C.L., Masyukova, S.V. and Yoder, B.K. (2010) Normal ciliogenesis requires synergy between the cystic kidney disease genes MKS-3 and NPHP-4. *JASN*, **21**, 782–793.
6. Masyukova, S.V., Winkelbauer, M.E., Williams, C.L., Pieczynski, J.N. and Yoder, B.K. (2011) Assessing the pathogenic potential of human nephronophthisis disease-associated NPHP-4 missense mutations in *C. elegans*. *Hum. Mol. Genet.*, **20**, 2942–2954.
7. Williams, C.L., Li, C., Kida, K., Inglis, P.N., Mohan, S., Semenec, L., Bialas, N.J., Stupay, R.M., Chen, N., Blacque, O.E. *et al.* (2011) MKS and NPHP modules cooperate to establish basal body/transition zone membrane associations and ciliary gate function during ciliogenesis. *J. Cell Biol.*, **192**, 1023–1041.
8. Warburton-Pitt, S.R.F., Jauregui, A.R., Li, C., Wang, J., Leroux, M.R. and Barr, M.M. (2012) Ciliogenesis in *Caenorhabditis elegans* requires genetic interactions between ciliary middle segment localized NPHP-2 (inversin) and transition zone-associated proteins. *J. Cell Sci.*, **125**, 2592–2603.
9. Hildebrandt, F., Otto, E., Rensing, C., Nothwang, H.G., Vollmer, M., Adolphs, J., Hanusch, H. and Brandis, M. (1997) A novel gene

encoding an SH3 domain protein is mutated in nephronophthisis type 1. *Nat. Genet.*, **17**, 149–153.
10. Jiang, S.-T., Chiou, Y.-Y., Wang, E., Lin, H.-K., Lee, S.-P., Lu, H.-Y., Wang, C.-K.L., Tang, M.-J. and Li, H. (2008) Targeted disruption of Nphp1 causes male infertility due to defects in the later steps of sperm morphogenesis in mice. *Hum. Mol. Genet.*, **17**, 3368–3379.
11. Won, J., Marín de Evsikova, C., Smith, R.S., Hicks, W.L., Edwards, M.M., Longo-Guess, C., Li, T., Naggert, J.K. and Nishina, P.M. (2011) NPHP4 is necessary for normal photoreceptor ribbon synapse maintenance and outer segment formation, and for sperm development. *Hum. Mol. Genet.*, **20**, 482–496.
12. Arts, H.H., Doherty, D., van Beersum, S.E.C., Parisi, M.A., Letteboer, S.J.F., Gorden, N.T., Peters, T.A., Märker, T., Voesenek, K., Kartono, A. *et al.* (2007) Mutations in the gene encoding the basal body protein RPGRIP1L, a nephrocystin-4 interactor, cause Joubert syndrome. *Nat. Genet.*, **39**, 882–888.
13. Delous, M., Baala, L., Salomon, R., Laclef, C., Vierkotten, J., Tory, K., Golzio, C., Lacoste, T., Besse, L., Ozilou, C. *et al.* (2007) The ciliary gene RPGRIP1L is mutated in cerebello-oculo-renal syndrome (Joubert syndrome type B) and Meckel syndrome. *Nat. Genet.*, **39**, 875–881.
14. Vierkotten, J., Dildrop, R., Peters, T., Wang, B. and Rüther, U. (2007) Ftm is a novel basal body protein of cilia involved in Shh signalling. *Development*, **134**, 2569–2577.
15. Richards, J. and Gumz, M.L. (2012) Advances in understanding the peripheral circadian clocks. *FASEB J.*, **26**, 3602–3613.
16. Olaoye, O.A., Masten, S.H., Mohandas, R. and Gumz, M.L. (2019) Circadian clock genes in diabetic kidney disease (DKD). *Curr. Diab. Rep.*, **19**, 42.
17. Partch, C.L., Green, C.B. and Takahashi, J.S. (2014) Molecular architecture of the mammalian circadian clock. *Trends Cell Biol.*, **24**, 90–99.
18. Pizarro, A., Hayer, K., Lahens, N.F. and Hogenesch, J.B. (2013) CircaDB: a database of mammalian circadian gene expression profiles. *Nucleic Acids Res.*, **41**, D1009–D1013.
19. Gava, A.L., Freitas, F.P., Balarini, C.M., Vasquez, E.C. and Meyrelles, S.S. (2012) Effects of 5/6 nephrectomy on renal function and blood pressure in mice. *Int. J. Physiol. Pathophysiol. Pharmacol.*, **4**, 167–173.
20. Polónia, J., Diogo, D., Caupers, P. and Damasceno, A. (2003) Influence of two doses of irbesartan on non-dipper circadian blood pressure rhythm in salt-sensitive black hypertensives under high salt diet. *J. Cardiovasc. Pharmacol.*, **42**, 98–104.
21. Huang, X.-M., Chen, W.-L., Yuan, J.-P., Yang, Y.-H., Mei, Q.-H. and Huang, L.-X. (2013) Altered diurnal variation and localization of clock proteins in the remnant kidney of 5/6 nephrectomy rats. *Nephrology (Carlton)*, **18**, 555–562.
22. Tokonami, N., Mordasini, D., Pradervand, S., Centeno, G., Jouffe, C., Maillard, M., Bonny, O., Gachon, F., Gomez, R.A., Sequeira-Lopez, M.L.S. *et al.* (2014) Local renal circadian clocks control fluid-electrolyte homeostasis and BP. *J. Am. Soc. Nephrol.*, **25**, 1430–1439.
23. Rossi, A., Kontarakis, Z., Gerri, C., Nolte, H., Hölper, S., Krüger, M. and Stainier, D.Y.R. (2015) Genetic compensation induced by deleterious mutations but not gene knockdowns. *Nature*, **524**, 230–233.
24. El-Brolosy, M.A. and Stainier, D.Y.R. (2017) Genetic compensation: a phenomenon in search of mechanisms. *PLoS Genet.*, **13**, e1006780.
25. El-Brolosy, M.A., Kontarakis, Z., Rossi, A., Kuenne, C., Günther, S., Fukuda, N., Kikhi, K., Boezio, G.L.M., Takacs, C.M., Lai, S.-L. *et al.* (2019) Genetic compensation triggered by mutant mRNA degradation. *Nature*, **568**, 193–197.
26. Love, M.I., Huber, W. and Anders, S. (2014) Moderated estimation of fold change and dispersion for RNA-seq data with DESeq2. *Genome Biol.*, **15**, 550.
27. Hirayama, J., Alifu, Y., Hamabe, R., Yamaguchi, S., Tomita, J., Maruyama, Y., Asaoka, Y., Nakahama, K.-I., Tamaru, T., Takamatsu, K. *et al.* (2019) The clock components Period2, Cryptochrome1a, and Cryptochrome2a function in establishing light-dependent behavioral rhythms and/or total activity levels in zebrafish. *Sci. Rep.*, **9**, 196.
28. Hirayama, J., Miyamura, N., Uchida, Y., Asaoka, Y., Honda, R., Sawanobori, K., Todo, T., Yamamoto, T., Sassone-Corsi, P. and Nishina, H. (2009) Common light signaling pathways controlling DNA repair and circadian clock entrainment in zebrafish. *Cell Cycle*, **8**, 2794–2801.
29. Burcklé, C., Gaudé, H.-M., Vesque, C., Silbermann, F., Salomon, R., Jeanpierre, C., Antignac, C., Saunier, S. and Schneider-Maunoury, S. (2011) Control of the Wnt pathways by nephrocystin-4 is required for morphogenesis of the zebrafish pronephros. *Hum. Mol. Genet.*, **20**, 2611–2627.
30. Slanchev, K., Pütz, M., Schmitt, A., Kramer-Zucker, A. and Walz, G. (2011) Nephrocystin-4 is required for pronephric duct-dependent cloaca formation in zebrafish. *Hum. Mol. Genet.*, **20**, 3119–3128.
31. Otto, E., Hoefele, J., Ruf, R., Mueller, A.M., Hiller, K.S., Wolf, M.T.F., Schuermann, M.J., Becker, A., Birkenhäger, R., Sudbrak, R. *et al.* (2002) A gene mutated in nephronophthisis and retinitis pigmentosa encodes a novel protein, nephroretinin, conserved in evolution. *Am. J. Hum. Genet.*, **71**, 1161–1167.
32. Stratigopoulos, G., Martin Carli, J.F., O'Day, D.R., Wang, L., Leduc, C.A., Lanzano, P., Chung, W.K., Rosenbaum, M., Egli, D., Doherty, D.A. *et al.* (2014) Hypomorphism for RPGRIP1L, a ciliary gene vicinal to the FTO locus, causes increased adiposity in mice. *Cell Metab.*, **19**, 767–779.
33. Stratigopoulos, G., Burnett, L.C., Rausch, R., Gill, R., Penn, D.B., Skowronski, A.A., LeDuc, C.A., Lanzano, A.J., Zhang, P., Storm, D.R. *et al.* (2016) Hypomorphism of Fto and Rpgrip1l causes obesity in mice. *J. Clin. Invest.*, **126**, 1897–1910.
34. Carli, J.F.M., LeDuc, C.A., Zhang, Y., Stratigopoulos, G. and Leibel, R.L. (2018) The role of Rpgrip1l, a component of the primary cilium, in adipocyte development and function. *FASEB J.*, **32**, 3946–3956.
35. Wang, L., De Solis, A.J., Goffer, Y., Birkenbach, K.E., Engle, S.E., Tanis, R., Levenson, J.M., Li, X., Rausch, R., Purohit, M. *et al.* (2019) Ciliary gene RPGRIP1L is required for hypothalamic arcuate neuron development. *JCI Insight*, **4**, 123337.
36. Doi, M., Takahashi, Y., Komatsu, R., Yamazaki, F., Yamada, H., Haraguchi, S., Emoto, N., Okuno, Y., Tsujimoto, G., Kanematsu, A. *et al.* (2010) Salt-sensitive hypertension in circadian clock-deficient Cry-null mice involves dysregulated adrenal Hsd3b6. *Nat. Med.*, **16**, 67–74.
37. Gumz, M.L., Stow, L.R., Lynch, I.J., Greenlee, M.M., Rudin, A., Cain, B.D., Weaver, D.R. and Wingo, C.S. (2009) The circadian clock protein Period 1 regulates expression of the renal epithelial sodium channel in mice. *J. Clin. Invest.*, **119**, 2423–2434.
38. Richards, J., Jeffers, L.A., All, S.C., Cheng, K.-Y. and Gumz, M.L. (2013) Role of Per1 and the mineralocorticoid receptor in the coordinate regulation of αENaC in renal cortical collecting duct cells. *Front. Physiol.*, **4**, 253.
39. Richards, J., Ko, B., All, S., Cheng, K.-Y., Hoover, R.S. and Gumz, M.L. (2014) A role for the circadian clock protein Per1 in the regulation of the NaCl co-transporter (NCC) and the with-no-lysine kinase (WNK) cascade in mouse distal convoluted tubule cells. *J. Biol. Chem.*, **289**, 11791–11806.

40. Richards, J., Welch, A.K., Barilovits, S.J., All, S., Cheng, K.-Y., Wingo, C.S., Cain, B.D. and Gumz, M.L. (2014) Tissue-specific and time-dependent regulation of the endothelin axis by the circadian clock protein Per1. *Life Sci.*, **118**, 255–262.
41. Gumz, M.L., Cheng, K.-Y., Lynch, I.J., Stow, L.R., Greenlee, M.M., Cain, B.D. and Wingo, C.S. (2010) Regulation of αENaC expression by the circadian clock protein Period 1 in mpkCCD(c14) cells. *Biochim. Biophys. Acta*, **1799**, 622–629.
42. Solocinski, K., Holzworth, M., Wen, X., Cheng, K.-Y., Lynch, I.J., Cain, B.D., Wingo, C.S. and Gumz, M.L. (2017) Desoxycorticosterone pivalate-salt treatment leads to non-dipping hypertension in Per1 knockout mice. *Acta Physiol (Oxf.)*, **220**, 72–82.
43. Olbrich, H., Fliegauf, M., Hoefele, J., Kispert, A., Otto, E., Volz, A., Wolf, M.T., Sasmaz, G., Trauer, U., Reinhardt, R. *et al.* (2003) Mutations in a novel gene, NPHP3, cause adolescent nephronophthisis, tapeto-retinal degeneration and hepatic fibrosis. *Nat. Genet.*, **34**, 455–459.
44. Otto, E.A., Schermer, B., Obara, T., O'Toole, J.F., Hiller, K.S., Mueller, A.M., Ruf, R.G., Hoefele, J., Beekmann, F., Landau, D. *et al.* (2003) Mutations in INVS encoding inversin cause nephronophthisis type 2, linking renal cystic disease to the function of primary cilia and left-right axis determination. *Nat. Genet.*, **34**, 413–420.
45. Sayer, J.A., Otto, E.A., O'Toole, J.F., Nurnberg, G., Kennedy, M.A., Becker, C., Hennies, H.C., Helou, J., Attanasio, M., Fausett, B.V. *et al.* (2006) The centrosomal protein nephrocystin-6 is mutated in Joubert syndrome and activates transcription factor ATF4. *Nat. Genet.*, **38**, 674–681.
46. Valente, E.M., Logan, C.V., Mougou-Zerelli, S., Lee, J.H., Silhavy, J.L., Brancati, F., Iannicelli, M., Travaglini, L., Romani, S., Illi, B. *et al.* (2010) Mutations in TMEM216 perturb ciliogenesis and cause Joubert, Meckel and related syndromes. *Nat. Genet.*, **42**, 619–625.
47. Chaki, M., Airik, R., Ghosh, A.K., Giles, R.H., Chen, R., Slaats, G.G., Wang, H., Hurd, T.W., Zhou, W., Cluckey, A. *et al.* (2012) Exome capture reveals ZNF423 and CEP164 mutations, linking renal ciliopathies to DNA damage response signaling. *Cell*, **150**, 533–548.
48. Hoff, S., Halbritter, J., Epting, D., Frank, V., Nguyen, T.-M.T., van Reeuwijk, J., Boehlke, C., Schell, C., Yasunaga, T., Helmstädter, M. *et al.* (2013) ANKS6 is a central component of a nephronophthisis module linking NEK8 to INVS and NPHP3. *Nat. Genet.*, **45**, 951–956.
49. Slaats, G.G., Ghosh, A.K., Falke, L.L., Le Corre, S., Shaltiel, I.A., van de Hoek, G., Klasson, T.D., Stokman, M.F., Logister, I., Verhaar, M.C. *et al.* (2014) Nephronophthisis-associated CEP164 regulates cell cycle progression, apoptosis and epithelial-to-mesenchymal transition. *PLoS Genet.*, **10**, e1004594.
50. Choi, Y.J., Halbritter, J., Braun, D.A., Schueler, M., Schapiro, D., Rim, J.H., Nandadasa, S., Choi, W.-I., Widmeier, E., Shril, S. *et al.* (2019) Mutations of ADAMTS9 cause nephronophthisis-related ciliopathy. *Am. J. Hum. Genet.*, **104**, 45–54.
51. Molinari, E., Ramsbottom, S.A., Sammut, V., Hughes, F.E.P. and Sayer, J.A. (2018) Using zebrafish to study the function of nephronophthisis and related ciliopathy genes. *F1000Res*, **7**, 1133.
52. Westerfield, M. (1995) The zebrafish book: a guide for the laboratory use of zebrafish. In Westerfield, M. (ed), *The Zebrafish Book: A Guide for the Laboratory Use of Zebrafish*, 3rd edn. Eugene, OR, University of Oregon Press, 385.
53. Yakulov, T.A., Todkar, A.P., Slanchev, K., Wiegel, J., Bona, A., Groß, M., Scholz, A., Hess, I., Wurditsch, A., Grahammer, F. *et al.* (2018) CXCL12 and MYC control energy metabolism to support adaptive responses after kidney injury. *Nat. Commun.*, **9**, 3660.
54. Labun, K., Montague, T.G., Gagnon, J.A., Thyme, S.B. and Valen, E. (2016) CHOPCHOP v2: a web tool for the next generation of CRISPR genome engineering. *Nucleic Acids Res.*, **44**, W272–W276.
55. Nakayama, T., Blitz, I.L., Fish, M.B., Odeleye, A.O., Manohar, S., Cho, K.W.Y. and Grainger, R.M. (2014) Cas9-based genome editing in *Xenopus tropicalis*. *Methods Enzymol.*, **546**, 355–375.
56. Robu, M.E., Larson, J.D., Nasevicius, A., Beiraghi, S., Brenner, C., Farber, S.A. and Ekker, S.C. (2007) p53 Activation by knockdown technologies. *PLoS Genet.*, **3**, e78.
57. Khanna, H., Davis, E.E., Murga-Zamalloa, C.A., Estrada-Cuzcano, A., Lopez, I., den Hollander, A.I., Zonneveld, M.N., Othman, M.I., Waseem, N., Chakarova, C.F. *et al.* (2009) A common allele in RPGRIP1L is a modifier of retinal degeneration in ciliopathies. *Nat. Genet.*, **41**, 739–745.
58. Schindelin, J., Arganda-Carreras, I., Frise, E., Kaynig, V., Longair, M., Pietzsch, T., Preibisch, S., Rueden, C., Saalfeld, S., Schmid, B. *et al.* (2012) Fiji: an open-source platform for biological-image analysis. *Nat. Methods*, **9**, 676–682.
59. Schoels, M., Zhuang, M., Fahrner, A., Küchlin, S., Sagar, H.F., Schmitt, A., Walz, G. and Yakulov, T.A. (2021) Single-cell mRNA profiling reveals changes in solute carrier expression and suggests a metabolic switch during zebrafish pronephros development. *Am. J. Physiol. Renal Physiol.*, **320**, F826–F837.
60. Dobin, A., Davis, C.A., Schlesinger, F., Drenkow, J., Zaleski, C., Jha, S., Batut, P., Chaisson, M. and Gingeras, T.R. (2013) STAR: ultrafast universal RNA-seq aligner. *Bioinformatics*, **29**, 15–21.
61. Li, B. and Dewey, C.N. (2011) RSEM: accurate transcript quantification from RNA-Seq data with or without a reference genome. *BMC Bioinformatics*, **12**, 323.
62. Robinson, J.T., Thorvaldsdóttir, H., Wenger, A.M., Zehir, A. and Mesirov, J.P. (2017) Variant review with the integrative genomics viewer. *Cancer Res.*, **77**, e31–e34.